Crystallization and amorphization studies of a $Ge_2Sb_{2.3}Te_5$ thin-film sample under pulsed laser irradiation

Pramod K. Khulbe, Xiaodong Xun, and M. Mansuripur

We present the results of crystallization and amorphization studies on a thin-film sample of $Ge_2Sb_{2.3}Te_5$, encapsulated in a quadrilayer stack as in the media of phase-change optical disk data storage. The study was conducted on a two-laser static tester in which one laser, operating in pulsed mode, writes either amorphous marks on a crystalline film or crystalline marks on an amorphous film. The second laser, operating at low power in the cw mode, simultaneously monitors the progress of mark formation in terms of the variations of reflectivity both during the write pulse and in the subsequent cooling period. In addition to investigating some of the expected features associated with crystallization and amorphization, we noted certain curious phenomena during the mark-formation process. For example, at low-power pulsed illumination, which is insufficient to trigger the phase transition, there is a slight change in the reflectivity of the sample. This is believed to be caused by a reversible change in the complex refractive index of the $Ge_2Sb_{2.3}Te_5$ film in the course of heating above the ambient temperature. We also observed that the mark-formation process may continue for as long as 1 μs beyond the end of the write laser pulse. This effect is especially pronounced during amorphous mark formation under high-power, long-pulse illumination.

OCIS codes: 210.0210, 210.4810, 210.4770, 210.4590.

1. Introduction

In phase-change (PC) optical data storage, information bits are recorded as submicrometer-sized amorphous marks on a thin chalcogenide polycrystalline film. We can achieve this by raising the local temperature of the film above its melting point (T_{melt}) with a high-power, focused laser pulse and subsequently cooling the heated spot rapidly below the material's glass transition temperature (T_{glass}). These amorphous marks can be erased (i.e., recrystallized) by means of annealing above T_{glass} under a laser pulse of suitable power and duration. The amorphous-to-crystalline phase transformation is accompanied by a fairly large change in the optical constants of the material. When these films are sandwiched between dielectric layers and incorporated into a quadrilayer stack, the changes in their optical constants can be used (through optical interference) to create a significant change in a stack's amplitude–phase reflectivity that is suitable for optical readout of the stored information.[1,2]

Crystallization, melting, and amorphization processes in thin-film PC media are, therefore, of fundamental significance in the technology of optical recording. The following media characteristics are required by an optical storage system: rapid and stable phase transition between amorphous and crystalline states, large signal-to-noise ratio in readout, and recyclability in the sense that the media must undergo a large number of read–write–erase cycles without deterioration. A relatively low melting point is desirable to ensure that the material can be melted with the available laser power. A large change between the amorphous and the crystalline (complex) refractive indices of the PC film is needed to achieve a large readout signal.

Several material systems meet the above criteria, and some of them are currently in use in erasable optical data storage products. These include the class of AgInSbTe quaternary alloys and the GeSbTe ternary alloys. Crystallization and amorphization studies on these media have been reported in the past, where a single laser is used both to trigger and

The authors are with the Optical Sciences Center, University of Arizona, Tucson, Arizona 85721. P. Khulbe's e-mail address is pkkhulbe@u.arizona.edu.

Received 22 September 1999; revised manuscript received 18 January 2000.
0003-6935/00/142359-08$15.00/0

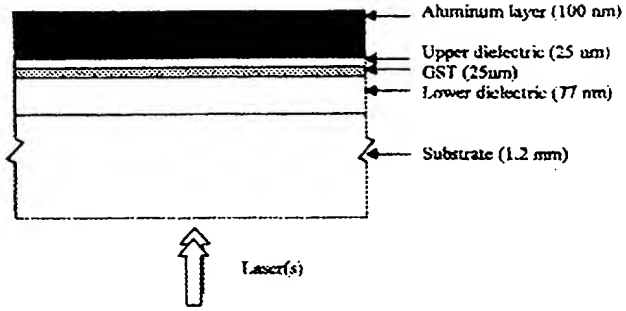

Fig. 1. Typical quadrilayer PC optical stack used for the study of crystallization and amorphization processes. The optical and the thermal constants of the various layers are listed in Table 1. The two laser beams are focused on the GST layer through the sample's substrate, and the microscope objective lens, which focuses the beams, is corrected for the 1.2-mm thickness of this substrate.

to monitor the process of phase transformation.[3–8] However, the single-laser scheme does not permit observations during the short time interval immediately following the rising and the falling edges of the laser pulse. In this paper we present time-resolved crystallization and amorphization data obtained on a two-laser static tester, believed to be new.[9] This system allows for continuous monitoring of the sample's reflectivity, starting prior to turning the write laser on and ending long after it has been turned off. We thus observe the behavior of the sample not only during the heating and the cooling periods but also in the vicinity of the rising and the falling edges of the writing pulse.

2. Sample and Static Tester

Figure 1 shows a typical quadrilayer PC optical disk structure, deposited on a 1.2-mm-thick polycarbonate substrate. The stack consists of a 77-nm-thick ZnS-SiO_2 lower dielectric layer, a 25-nm-thick $Ge_2Sb_{2.3}Te_5$ PC layer (hereafter referred to as GST), a 25-nm-thick ZnS-SiO_2 upper dielectric layer, and a 100-nm-thick aluminum alloy reflector layer. The lower dielectric layer protects the substrate against thermal damage by controlling the flux of heat toward the substrate. The upper dielectric layer optimizes the cooling rate of the PC film by adjusting heat flow toward the aluminum heat-sinking layer. The optical and the thermal properties of these layers (listed in Table 1) were taken into consideration in designing the structure of the stack, which provides optimum read, write, and overwrite sensitivities in a data storage system. The reflectivity and the absorption of the stack are adjusted by use of optical interference effects,[10,11] and the temperature profiles are tailored by balancing of lateral and vertical heat diffusion. At the operating wavelength of $\lambda = 643$ nm, the multilayer stack of Fig. 1 has reflectivity $R_a \sim 3\%$ when the GST layer is amorphous and $R_c \sim 20\%$ when the GST layer is fully crystalline.

Our crystallization and amorphization experiments on the quadrilayer sample were conducted with a two-laser static tester built around a commercial polarized-light microscope; details of the construction and functioning of the tester are given elsewhere.[9] A white-light source illuminates the field of view of the objective lens for visual inspection of the sample. The microscope is equipped with two semiconductor laser diodes operating at $\lambda_1 = 680$ nm (laser 1) and $\lambda_2 = 643$ nm (laser 2). For the measurements reported here we used laser 1 in pulsed mode and laser 2 in a low-power, cw mode ($P_2 = 0.2$ to 0.3 mW). Both lasers are focused simultaneously and coincidentally on the PC layer of the sample through a 0.6-N.A. objective lens, corrected for the 1.2-mm thickness of the sample's substrate. The focused spot diameters (full-width at half-maximum intensity) are estimated at FWHM ~ 0.7 μm. The light reflected from the sample is collected by the same objective lens and sent through a glass prism, which separates the two laser beams and directs them toward individual photodetectors. The detector outputs are fed into a digital oscilloscope and a computer for further processing, where reflected signal can be averaged over multiple runs. All the reflectivity traces presented in this paper are averaged over 40 runs, each run conducted on a fresh spot on the sample under identical conditions.

The reflectance of the sample is calibrated against a polished silicon surface that has a nominal reflectivity of 33%. The silicon sample has a large thermal conductivity, and therefore its reflectance is not expected to change significantly as it absorbs the energy of the focused laser beam. Figure 2 shows measured plots of the photodetector's signal versus time for a 2-μs pulse of laser 1 at several values of the power P_1 incident on the silicon surface. The reflected pulses are seen to be fairly uniform throughout the pulse period, and their detected signal (in mV) is proportional to the value of P_1. In the following discussions the slight nonuniformity of the pulses observed in Fig. 2 will be ignored. For accurate comparisons of the experimental results with theoretical

Table 1. Optical and Thermal Constants of the Various Materials Used in the Calculations

	Refractive Index $n + ik$ ($\lambda = 680$ nm)	Specific Heat C (J/cm³/°C)	Thermal Conductivity K (J/cm/s/°C)
Polycarbonate (substrate)	1.58	1.70	0.0022
Aluminum alloy	$1.9 \pm i6.2$	2.45	0.400
$Ge_2Sb_2Te_5$ (amorphous)	$4.3 \pm i1.7$	1.30	0.002
$Ge_2Sb_2Te_5$ (polycrystal)	$4.8 \pm i4.2$	1.30	0.005
ZnS-SiO_2 (dielectric)	2.09	2.00	0.006

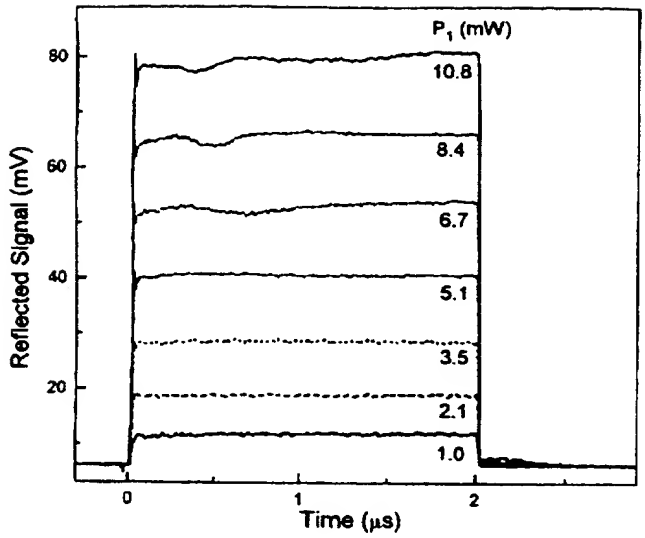

Fig. 2. Photodetector signals (in millivolts) versus time, measured with a 2-μs pulse from laser 1 reflecting off a polished silicon surface. The silicon sample has a nominal reflectivity of 33%. Different plots correspond to different values of the laser power P_1 incident on the sample's surface. There is ~6.2 mV of added background signal inherent in these measurements, owing to the offset voltage of the detector amplifier.

calculations, however, these nonuniform pulse shapes must be introduced directly into the computer simulations.

3. Crystallization Experiments

Figure 3 shows the variations in reflectivity R caused by crystalline mark formation on an as-deposited amorphous film under a 2-μs rectangular pulse at various power levels of laser 1 (P_1 = 2.1–11.2 mW). These reflectivity variations are monitored during and after the pulse of laser 1 with the help of laser 2, which operates in the cw mode at $P_2 \sim 0.2$ mW. This value of P_2 is small enough for its thermal effects on the sample to be ignored. For all the values of P_1 examined, R starts at the amorphous-state reflectivity $R_a \sim 2.5\%$ and, once the pulse is triggered, drops a little in the beginning before it starts rising toward the crystalline-state reflectivity $R_c \sim 20\%$. The traces in Fig. 3 have been vertically shifted by an arbitrary amount for clarity of presentation.

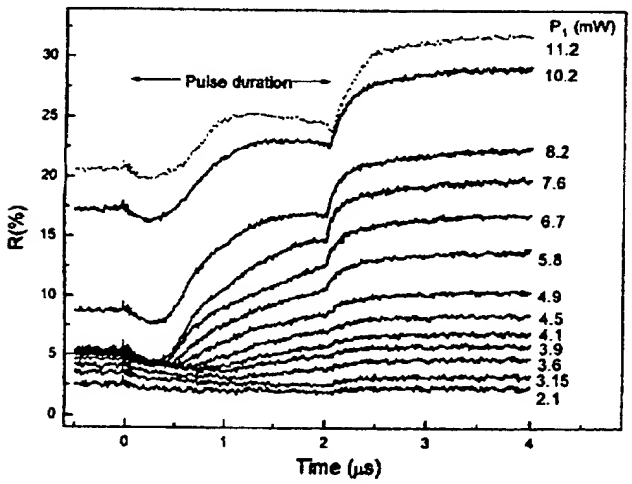

Fig. 3. Reflectivity variations during crystallization of the as-deposited GST film in the quadrilayer stack of Fig. 1. Different curves correspond to different values of the laser pulse power P_1, as indicated on the right-hand side of each curve. The pulse duration was 2 μs, and the monitoring cw laser power P_2 was 0.2 mW. For ease of presentation the curves have been vertically displaced by arbitrary amounts from an original position where $R(0) = R_a \sim 3\%$.

At the start of the pulse, reflectivity drops by as much as 1% in the early stage of the heating cycle. This drop is believed to be caused by variations in the optical constants of the PC layer with the rising temperature; we will see that this initial drop in R is reversible. With the onset of crystallization at the center of the focused spot, which has the highest temperature, reflectivity begins to increase. The crystalline mark grows outward from the center of the focused spot, and reflectivity increases first rapidly, then at a slower rate. The reflectivity at the end of the pulse does not reach its crystallized-state value, because the final crystalline mark always remains smaller than the focused spot. When $P_1 <$ 3.15 mW, no crystallization is observed within the 2-μs period of the pulse. In these curves the small monotonic drop in R during the pulse and the subsequent rise immediately afterward are likely to be manifestations of a temperature dependence of the optical constants of the PC layer. At $P_1 > 3.15$ mW the time to crystallization onset (t_{onset}) decreases nonlinearly with an increase of P_1 up to ~ 7.6 mW. For $P_1 > 7.6$ mW, t_{onset} becomes almost constant at ~300 ns. The crystallization rate (or the average rate of change in reflectivity, $\Delta R/\Delta t$) increases as P_1 is raised from 3.15 to 7.6 mW. At $P_1 = 7.6$ mW, R saturates at the end of the pulse.

On further increasing P_1, we observe a drop in R toward the end of the pulse. This drop is due to the melting of the GST film at the center of the focused spot. At higher values of P_1 the temperature of the PC layer at the center of the spot exceeds T_{melt} during the pulse. Thus a molten pool appears at the center, which grows in time. Simultaneously with this melting, crystal growth continues at the periphery of the hot spot. The net change in R is thus the sum of contributions from the central melt and the surrounding crystalline ring. If P_1 is increased beyond a certain point, there will be a large molten pool at the center, whose contribution will dominate the overall reflectivity of the sample.

The reflectivity measured (by laser 2) after the end of the write pulse gives information about the cooling behavior of the hot spot. In Fig. 3 we observe a rapid rise in reflectivity immediately after the end of the write pulse, followed by a relatively slow increase. A small contribution to this rise in R is due to the return of the optical constants to their room-temperature values as the sample cools. However, the major contribution comes from partial recrystallization of the

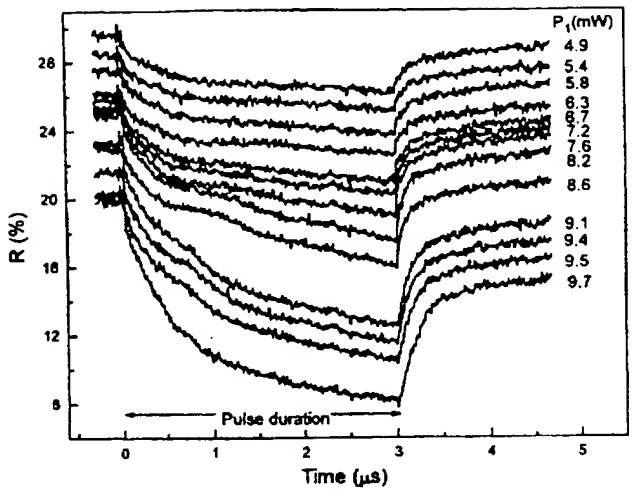

Fig. 4. Reflectivity variations during melting and subsequent amorphization of the GST film in the quadrilayer stack of Fig. 1. Different curves correspond to different values of the laser pulse power P_1, as indicated on the right-hand side of each curve. The pulse duration was 3 μs, and the monitoring cw laser power P_2 was 0.3 mW. For ease of presentation the curves have been vertically displaced by arbitrary amounts from an original position where $R(0) = R_c \sim 20\%$.

central melt. The small increase in R at the end of the pulse for $P_1 \leq 4.9$ mW, where no melting is expected, is due to the former effect. The hot spot at the end of the pulse, whose cooling gives rise to this increase in reflectivity, enlarges with the increasing pulse power and pulse duration, because of the lateral heat diffusion. Thus cooling of a larger spot should contribute more to the rise in R at the end of the pulse. Below we will see that the variation with temperature of optical constants is larger for the crystalline state of the PC film than for its amorphous state. At high powers ($P_1 \geq 5.8$ mW) partial recrystallization of the central melt, starting from the periphery and moving inward, contributes substantially to the increase in R during the cooling period. Because the central melt is larger at higher pulse powers, we observe a larger increase in R at the end of the pulse as P_1 is increased from 5.8 to 11.2 mW.

4. Melting Experiments

We conducted melting and amorphization experiments on the sample depicted in Fig. 1, starting from a crystalline state of the GST layer. At first a large section of the sample was crystallized by a slow XY scan under a cw laser beam operating at ~2.0 mW. Then, to melt the sample locally (i.e., under the focused laser beam), we used a 3.0-μs-long rectangular pulse from laser 1 at various power levels ranging from 4.9 to 9.7 mW. For 4.5 μs from the beginning of the pulse, the melting–amorphization process was monitored by laser 2 operating in the cw mode at $P_2 \sim 0.3$ mW, as shown in Fig. 4. For any given value of P_1 the reflectivity starts at $R_c \sim 20\%$ (the curves in Fig. 4 have been shifted vertically for clarity of presentation). As long as $P_1 < 6.7$ mW, there is a reversible drop in R, which means that the crystalline-state reflectivity recovers once the write pulse is turned off and that there is no melt (amorphous) mark formation. This is probably caused by a reversible change in the optical constants of the sample with the rising temperature, as mentioned above. It seems that for the pulse power $P_1 < 6.7$ mW there is no melting. For $P_1 > 6.7$ mW the temperature of the GST film at the center of the laser spot exceeds the melting point temperature, which brings a permanent change in reflectivity. For higher values of P_1, R decreases further, first rapidly, then at a slower rate. The time to onset of melting is expected to become shorter for larger values of P_1. Below ~6.7 mW, no melting is observed for any pulse duration.

For all values of P_1, reflectivity increases rapidly immediately after the end of the pulse. This increase in R brings the reflectivity back to its fully crystalline value for $P_1 \leq 6.7$ mW, where there appears to be no melting. For $P_1 > 6.7$ mW, there is greater gain in R at the end of the pulse for larger values of P_1, indicating the shrinkage of a larger central molten region by inward growth of its crystalline boundary.

5. Melting Onset

From the reflectivity traces of Fig. 4, obtained during melting and the subsequent amorphous mark formation, it is difficult to determine the time to melting onset, t_{onset}. This difficulty in determining t_{onset} is due to the rapid initial drop in R, which occurs in the beginning of the pulse and has nothing to do with melting, followed by a featureless, monotonic decline after the onset of melting. To determine t_{onset}, we conducted another experiment in which the pulse duration was systematically increased for a given value of P_1, until it caused a perceptible permanent drop in R. This shortest required pulse width was assigned to t_{onset} for the given value of P_1. Such measurements were carried out for 8 mW $< P_1 <$ 15 mW, and the results are presented in Fig. 5 (squares).

The measured values of t_{onset} shown in Fig. 5 were used to estimate the thermal conductivity K of the various layers of the stack, under the assumption that, at t_{onset}, the temperature of the GST layer at the center of the focused spot must have reached $T_{melt} \sim$ 620 °C. The optical constants of the layers were determined from ellipsometry, and the specific heat values were estimated on the basis of differential scanning calorimetry on bulk samples. The only adjustable parameters in our calculations, therefore, were the thermal conductivity (K) values of the various layers of the stack. In these calculations the material parameters were fixed over the entire temperature range. Several conductivity values for the dielectric, aluminum, and GST layers were chosen to fit the measured data. The dashed curve in Fig. 5 shows the theoretically obtained values of t_{onset} versus P_1, in excellent agreement with the experimental data. The numerical calculations were performed with the program TEMPROFILE[12] with the param-

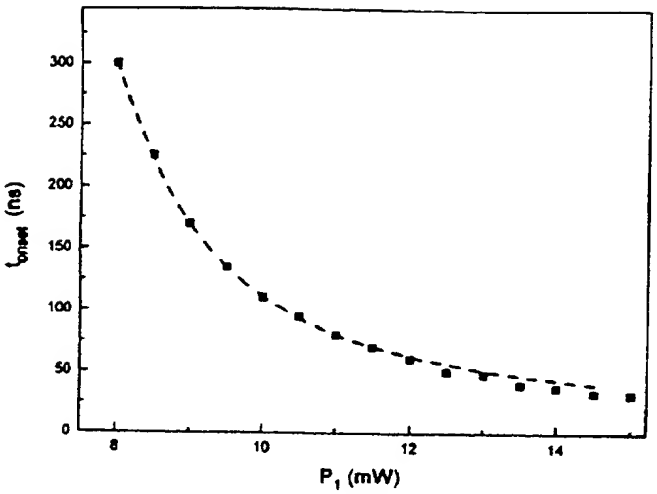

Fig. 5. Onset time of melting, t_{onset}, in the crystalline GST film versus the laser pulse power P_1. Squares are experimental data points, and the dashed curve is obtained by computer simulations in which the values of the thermal conductivity K of the various layers were adjusted to achieve a good match to the measured data. These values of K are listed in Table 1.

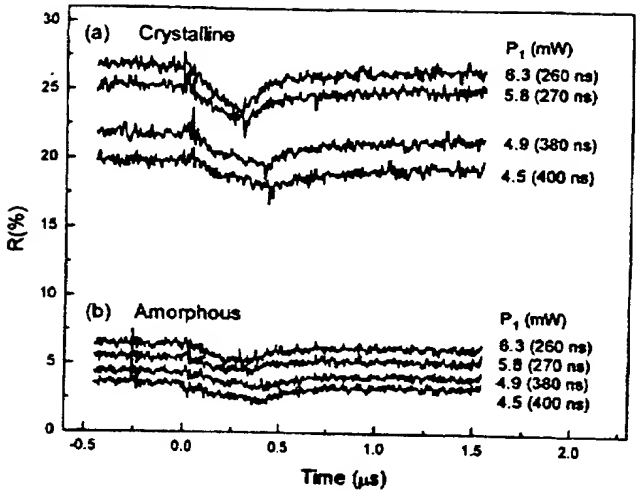

Fig. 6. Reversible changes occur in the reflectivity of the quadrilayer stack of Fig. 1 under laser heating with a short, relatively low-power pulse prior to the onset of phase transformation. In (a) the GST film is crystallized, whereas in (b) it is in the as-deposited amorphous state. For ease of presentation the curves have been vertically displaced by arbitrary amounts from their original positions. The corresponding pulse power and pulse duration is shown on the right-hand side of each curve.

eters listed in Table 1. Because in our approach there is no unique way of arriving at the K values, it is conceivable that another set of values can be found to match the experimental data. However, in light of the difficulty of obtaining a good match over a wide range of measurements, we believe that the estimated values of K listed in Table 1 are realistic.

6. Reversible Changes of Reflectivity

Using pulses shorter than the crystallization and amorphization onset times for the corresponding pulse power, we verified the reversibility of the initial drop in R, observed during both crystallization and melting experiments depicted in Figs. 3 and 4, respectively. We fired 41 such pulses at the same spot of the GST film, and the time-based reflectivity signal, measured by laser 2, was averaged over the final 40 incidents. The time interval between successive pulses was several seconds, long enough to allow for cooling of the spot after the preceding pulse. Such plots of reflectivity versus time, obtained for both amorphous and crystalline GST films, are shown in Fig. 6. These plots indicate that, as the laser pulse heats the sample locally, there is a drop in R without any phase transformation (or any other permanent change) and, when the laser is turned off, the reflectivity returns to its room-temperature value. In understanding this explanation it is important to remember that the individual reflectivity traces in Fig. 6 are averages of 40 traces obtained under identical laser pulses fired at the same spot of the film. If the first pulse had brought about a permanent change in the film, subsequent curves would have behaved differently, perhaps progressively so, and this change would have resulted in a perceptible difference between the first curve and the subsequent curves. In the absence of such differences we thus believe that the temperature dependence of the complex indices of refraction is responsible for the observed behavior. The results depicted in Fig. 6 also indicate that the reversible drop in R for crystalline samples is greater than that for the amorphous sample.

7. Long-Pulse Irradiation

In our preliminary experiments we noted that the crystallization and amorphization processes might continue for a while after the write pulse is turned off. To study this behavior further, we conducted several experiments with variable pulse duration. Figure 7 shows the reflectivity traces taken during the crystallization of an as-deposited amorphous film with different laser pulse widths (in the range of 0.25–4.0 μs) at P_1 = 5.0 mW. In each trace the end of the pulse is easy to recognize, because it corresponds to a sharp change of slope in the reflectivity-versus-time plot. In Fig. 8 we show the net reflectivity gain ΔR during the cooling period as a function of the pulse width, obtained in crystallization experiments similar to those depicted in Fig. 7. It is evident that, after turning off the pulse, there is more crystallization with longer pulses. We must keep in mind, however, that a fraction of ΔR in Fig. 8 is due to the index change with temperature.

Similar experiments were done on a precrystallized sample, which led to melting followed by amorphous mark formation. A typical set of reflectivity-versus-time traces corresponding to P_1 = 9.0 mW for various pulse widths (ranging from 0.5 to 4.0 μs) are shown in Fig. 9. The general behavior of each trace is similar to those of Fig. 4, the noteworthy feature being the relatively large increase in R at the end of the longer

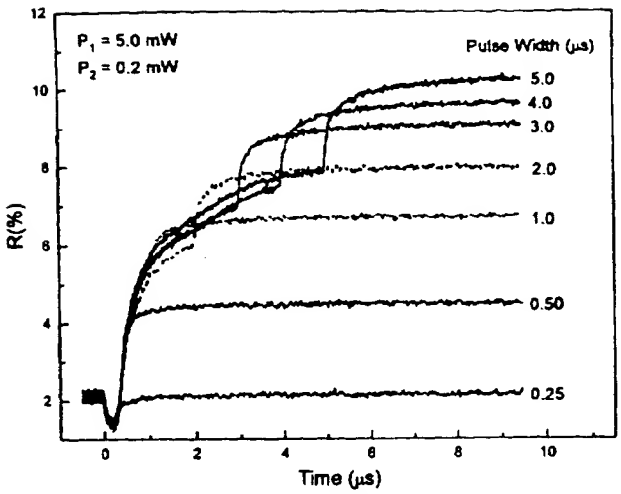

Fig. 7. Variations of reflectivity with time during crystallization of the as-deposited GST film under a focused laser beam with different pulse widths, ranging from 0.5 to 4.5 μs, at P_1 = 5.0 mW. The monitoring cw laser power P_2 = 0.2 mW.

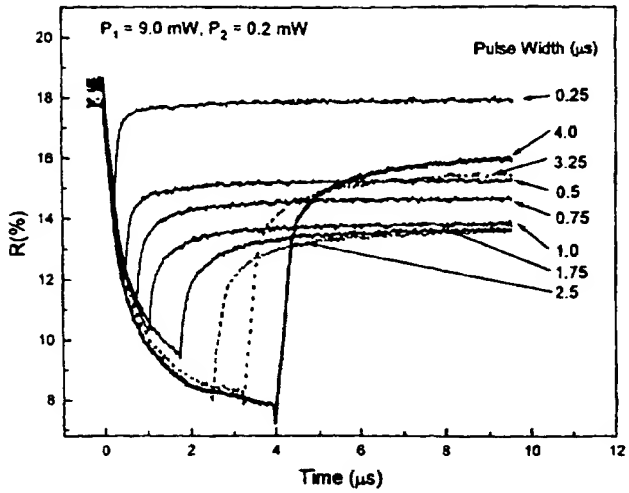

Fig. 9. Variations of reflectivity with time during melting and subsequent amorphization of a precrystallized GST film under a focused laser beam with different pulse widths, ranging from 0.5 to 4.0 μs, at P_1 = 9.0 mW. The monitoring cw laser power P_2 = 0.2 mW.

pulses. Figure 10(a) shows the net ΔR during the cooling period as function of the pulse width for various values of P_1. It is clear that, below ~1.5 μs, ΔR is essentially constant for each value of P_1. Thereafter it continually increases with the pulse width. It seems that beyond t = 1.5 μs the temperature at the center of the melt is more or less constant and that thermal diffusion overtakes the process of heating by light absorption. This slows down the cooling rate at the melt boundary when the pulse is turned off, thus providing sufficient time for recrystallization, which starts at the boundary and moves inward.

For the same experiments as exemplified by Fig. 9 we show in Fig. 10(b) plots of $R(0) - R(\infty)$ versus pulse width at various laser powers, $R(0) - R(\infty)$ being the total loss of reflectivity during amorphous mark formation [i.e., the difference between crystalline-state reflectivity $R(0)=R_c$ and the final reflectivity $R(\infty)$ from the recorded mark after complete cooldown]. This figure clearly indicates the existence of an optimum pulse duration for writing the largest amorphous mark at a given pulse power P_1.

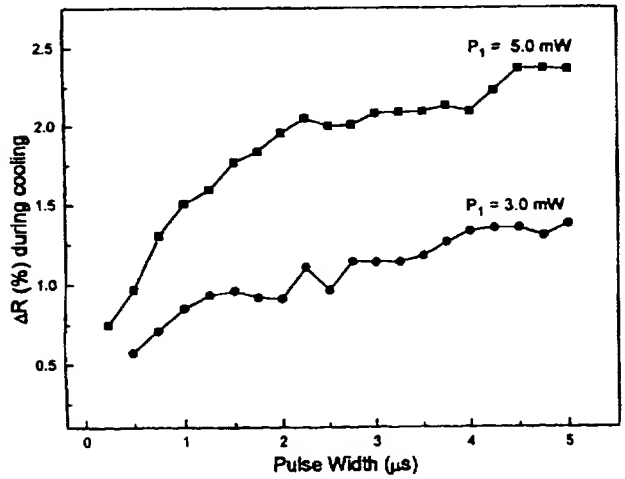

Fig. 8. Net gain in reflectivity ΔR during the cooling period as function of the pulse width obtained in experiments of the type depicted in Fig. 7. The as-deposited amorphous film is started on its crystallization path by a laser pulse of varying duration at a power level of P_1 = 3.0 mW (circles) or P_1 = 5.0 mW (squares).

To understand the recrystallization behavior during cooldown from melt, we ought to look at the nature of heat diffusion in the multilayer stack. Early in the laser pulse, temperatures in the GST film at the center of the spot rise rapidly because of strong light absorption in this region. With the increase of temperature, thermal diffusion becomes more and more significant along both axial and radial directions, balancing the rate of heating until equilibrium is established. The actual time to reach this thermal equilibrium depends on the structure of the multilayer stack as well as the optical and the thermal constants of the sample. Using the computer program TEMPROFILE[12] and ignoring the phase transitions, the heat of melting and of solidification, and the temperature dependence of the parameters, we computed the temperature profiles in the quadrilayer stack of Fig. 1 with the parameters listed in Table 1. Needless to say, these thermal calculations are based on overly simplified assumptions. The fact remains, however, that the numerical values of the optical and the thermal constants of the layers are available only at room temperature; even then, they are rough estimates at best. Also, good estimates of the heat of crystallization and of melting of the PC layer are presently unavailable. However, it is fortunate that the thermal mass of the sample consists mainly of the dielectric layers, the aluminum layer, and (for longer time in heating cycle) the substrate. Since the heat

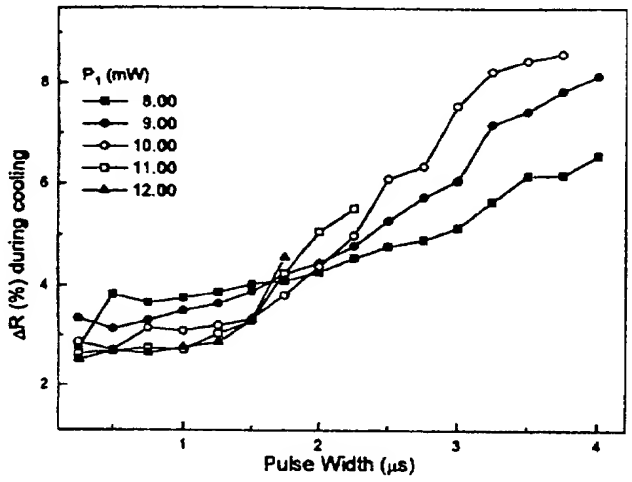

(a)

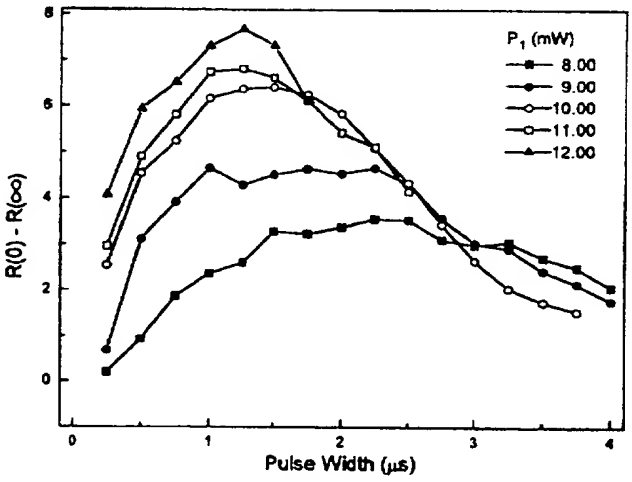

(b)

Fig. 10. Net change in reflectivity as function of the laser pulse width, observed in experiments of the type depicted in Fig. 9. The horizontal axis corresponds to pulse duration, and different symbols are used to represent different pulse magnitudes P_1. (a) Net reflectivity gain ΔR during the cooling period. The vertical axis shows the change in R between the end of the pulse and $t = 10$ μs. (b) Loss of reflectivity $[R(0) - R(\infty)]$ between the beginning of the pulse, when the sample is fully crystallized, and $t = 10$ μs, when the writing is essentially complete.

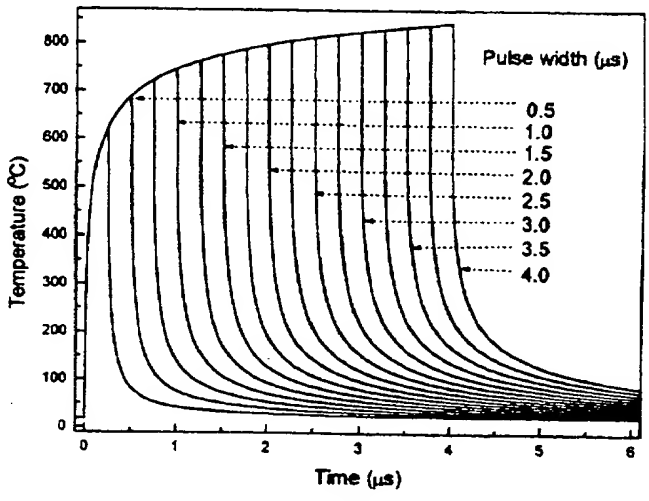

(a)

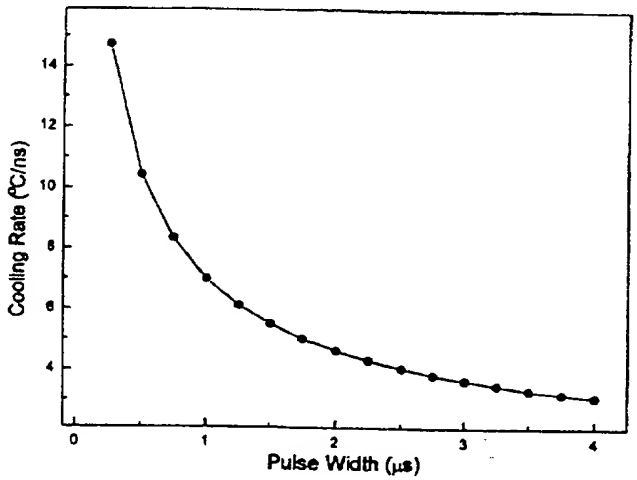

(b)

Fig. 11. (a) Computed profiles of temperature versus time in the GST film at the center of the focused spot at $P_1 = 8.0$ mW for various pulse durations. The simulated quadrilayer stack is depicted in Fig. 1, and its relevant optical and thermal parameters appear in Table 1. (b) The rate of decline of temperature with time in the GST film at the center of the spot immediately after turning off the write pulse. These cooling rates obtained from the temperature profiles in (a) indicate that, by creating a more homogeneous temperature distribution within the stack, a longer pulse causes a slowdown of the cooling process at the end of the pulse.

of crystallization and of melting are proportional to the thickness of the PC layer, which is relatively thin in our sample, their influence on the overall thermal profile may be safely ignored. In light of the above arguments, perhaps the best we can do is to ignore the aforementioned factors and simply treat the stack parameters as temperature independent. Obviously, the results thus obtained are meaningful only as a first approximation. The results of these calculations appear in Fig. 11(a), where the rise and the fall in times of the temperature of the GST film at the center of the focused spot are shown for various pulse widths ($P_1 = 8.0$ mW). The average cooling rate at the end of the pulse is extracted from the plots of Fig. 11(a) and is shown versus the pulse width in Fig. 11(b). This plot makes it amply clear that the cooling must proceed more slowly at the end of longer pulses. Away from the center of the focused spot the cooling rate will be even slower. Consequently, if the heated region spends more time in the temperature range of crystallization, it is likely that there will be more crystallization after turning off the pulse.

8. Conclusions

The variations of reflectivity during crystallization, melting, and amorphous mark formation in a typical

quadrilayer GST-based PC sample were presented and discussed for a range of laser pulse widths and pulse powers. Among other things, this study has revealed the following features of the crystallization and amorphization processes in GST films:

i. A minimum length of time is required for triggering the crystallization of the as-deposited amorphous film, suggesting that the formation of critical-size nuclei requires a minimum of incubation time, a standard concept in the theory of crystallization of solids.

ii. The complex refractive index of the GST film shows a slight variation with temperature. Depending on the structure of the sample, this variation could lead to either a decrease or an increase of reflectivity when the sample is heated below its crystallization temperature (in the case of an amorphous sample) or below its melting point (in the case of a crystalline sample).

iii. There are optimum values for the laser pulse power and duration for writing the largest possible amorphous mark on a given crystallized film. The structure as well as the optical and the thermal constants of the sample determine these optimum values.

This research was supported in part by the U.S. Department of Commerce through the National Storage Industry Consortium/Multiple Optical Recording Enhancements (NSIC/MORE) program (cooperative agreement 70NANB7H3054). The authors thank T. Ohta and K. Nagata of the Matsushita Electric Industries Corporation, Japan, for providing the PC samples for this study.

References and Note

1. T. Ide and M. Okada, "Jitter improvement in mark edge recording for phase-change optical disk with optical phase encoding," Appl. Phys. Lett. **64**, 1613–1614 (1994).
2. C. Peng, M. Mansuripur, W. M. Kim, and S. G. Kim, "Edge detection in phase-change optical data storage," Appl. Phys. Lett. **71**, 2088–2090 (1997).
3. J. H. Coombs, A. P. J. M. Jongenelis, W. van Es-Spiekman, and B. A. J. Jacobs, "Laser-induced crystallization phenomena in Ge-Te-based alloys. I. Characterization of nucleation and growth," J. Appl. Phys. **78**, 4906–4913 (1995).
4. T. Ohta, K. Nagata, I. Satoh, and R. Imanaka, "Overwritable phase-change optical disk recording," IEEE Trans. Magnet. **34**, 426–431 (1998).
5. K. Nishiuchi, N. Yamada, N. Akahira, M. Takenaga, and R. Akutagawa, "Laser diode beam exposure instrument for rapid quenching of thin-film material," Rev. Sci. Instrum. **63**, 3425–3430 (1992).
6. N. Yamada, E. Ohno, K. Nishiuchi, N. Akahira, and M. Takao, "Rapid-phase transition of GeTe-Sb_2Te_3 pseudobinary amorphous thin films for an optical disk memory," J. Appl. Phys. **69**, 2849–2856 (1991).
7. M. Chen, K. Rubin, and R. Barton, "Compound material for reversible, phase-change optical data storage," Appl. Phys. Lett. **49**, 502–504 (1986).
8. M. Chen, K. A. Rubin, V. Marrello, U. G. Gerber, and V. B. Jipson, "Reversibility and stability of tellurium alloys for optical data storage applications," Appl. Phys. Lett. **46**, 734–736 (1985).
9. M. Mansuripur, J. K. Erwin, W. Bletscher, P. Khulbe, K. Sadeghi, X. Xun, A. Gupta, and S. B. Mendes, "Static tester for characterization of phase-change, dye-polymer, and magneto-optical media for optical data storage," Appl. Opt. **38**, 7095–7104 (1999).
10. T. Ohta, N. Akahira, S. Ohara, and I. Satoh, "High-density phase-change optical recording," Optoelectron. Devices Technol. **10**, 361–380 (1995).
11. T. Ohta, "Study of phase-change optical disk memory," Ph.D. dissertation (Osaka Prefecture University, Osaka, Japan, 1995).
12. TEMPROFILE is a product of MM Research Inc., Tucson, Arizona. The theoretical basis of the program is described in M. Mansuripur, G. A. N. Connell, and J. W. Goodman, "Laser-induced local heating of multilayers," Appl. Opt. **21**, 1106–1114 (1982) and in M. Mansuripur and G. A. N. Connell, "Laser-induced local heating of moving multilayer media," Appl. Opt. **22**, 666–670 (1983).